J. Fluid Mech. (1990), *vol.* 220, *pp.* 459–484
Printed in Great Britain

Unsteady flow past a rotating circular cylinder at Reynolds numbers 10^3 and 10^4

By H. M. BADR[1], M. COUTANCEAU[2], S. C. R. DENNIS[3] AND C. MÉNARD[2]

[1] Department of Mechanical Engineering, King Fahd University of Petroleum and Minerals, Dhahran, Saudia Arabia

[2] Laboratoire de Mécanique des Fluides, 40 Avenue du Recteur Pineau, Poitiers 86022, France

[3] Department of Applied Mathematics, University of Western Ontario, London, Ontario, Canada N6A 5B9

(Received 20 July 1988 and in revised form 30 March 1990)

The unsteady flow past a circular cylinder which starts translating and rotating impulsively from rest in a viscous fluid is investigated both theoretically and experimentally in the Reynolds number range $10^3 \leqslant R \leqslant 10^4$ and for rotational to translational surface speed ratios between 0.5 and 3. The theoretical study is based on numerical solutions of the two-dimensional unsteady Navier–Stokes equations while the experimental investigation is based on visualization of the flow using very fine suspended particles. The object of the study is to examine the effect of increase of rotation on the flow structure. There is excellent agreement between the numerical and experimental results for all speed ratios considered, except in the case of the highest rotation rate. Here three-dimensional effects become more pronounced in the experiments and the laminar flow breaks down, while the calculated flow starts to approach a steady state. For lower rotation rates a periodic structure of vortex evolution and shedding develops in the calculations which is repeated exactly as time advances. Another feature of the calculations is the discrepancy in the lift and drag forces at high Reynolds numbers resulting from solving the boundary-layer limit of the equations of motion rather than the full Navier–Stokes equations. Typical results are given for selected values of the Reynolds number and rotation rate.

1. Introduction

This paper presents the results of a joint theoretical and experimental study of the unsteady flow generated in a viscous fluid by a circular cylinder which is impulsively started into a uniform translational motion normal to its axis and a uniform rotational motion about it. The fluid motion is two-dimensional and the theoretical results are based on numerical solutions of the Navier–Stokes equations for incompressible fluids. In the experimental study, the flow is generally two-dimensional except for the highest rotational rate of the cylinder, where the flow starts to develop three-dimensional and turbulent effects which appear at later times. In such cases, it is still possible to identify many common features of the experimental and calculated flows, particularly up to the time for which the flow continues to be laminar, and even beyond in some flow regions.

The flow field depends mainly on three parameters. The first is the Reynolds number $R = 2Ua/\nu$, where U is the constant speed of translation of the cylinder after its sudden start from rest, a is the radius of the cylinder and ν is the coefficient of

kinematic viscosity of the fluid. The second is the velocity ratio $\alpha = a\omega_0/U$, where ω_0 is the angular velocity of the cylinder about its axis. The third parameter is a suitably scaled time after the start of the motion, measured by $\tau = Ut/a$, where t is the actual time. In the present study we investigate a higher Reynolds-number range and higher speeds of rotation than those previously considered. In fact, no calculations of the unsteady flow exist for $\alpha > 1$ and our object is to examine the effect of increase of α on both the theoretical and experimental flow at a fixed, high enough, Reynolds number. Important changes in both flows take place as α increases and many features not previously reported appear, particularly with regard to the suppression of the separated vortex region.

The inhibition of vortex formation at higher rotational rates is of interest in view of the early investigations of flow past rotating cylinders. It is well known that the effect of imposing an increasing circulation on the potential flow past a fixed circular cylinder leads eventually to a flow pattern with closed streamlines surrounding the cylinder (Goldstein 1938, p. 33). A comparable situation exists in the experimental studies of the development with time of the flow past a rotating circular cylinder (Prandtl 1927; Prandtl & Tietjens 1931; see also Goldstein 1938, plates 15–18). Here the circulation is generated by the rotating cylinder itself and the motion of the surface inhibits separation of the flow. Theoretical studies of the steady flow have been made by Moore (1957), Glauert (1957*a*, *b*) and Wood (1957). These studies indicate that for high enough α it is possible to obtain steady flows with no vortex shedding for both high and low Reynolds numbers. However, these investigations were not based on the full Navier–Stokes equations of motion but rather on boundary-layer theory.

A boundary-layer analysis of the present problem has also been considered by Ece, Walker & Doligalski (1984) for the case of very high Reynolds numbers ($R \to \infty$) by simply setting $R = \infty$ in a boundary-layer formulation. Although the boundary-layer equations are in some ways easier to handle, the resulting solution does not represent in all aspects the situation at very high Reynolds number. For example, the exploded view of the streamline pattern given by Ece *et al.* would occupy a physical space covered by the entire surface of the cylinder but would have zero thickness when $R = \infty$. Moreover, the magnitude and the direction of the lift force predicted by the boundary-layer analysis is not the same as that obtained from the Navier–Stokes equations for very high Reynolds number. This is demonstrated in the present paper and some detailed results are provided.

Steady flows over rotating cylinders at small values of R and low rotation rates have been given by Loc (1975) and Ingham (1983) for $R = 5$, 20 and $0 \leqslant \alpha \leqslant 0.5$. A steady-state limit of the solution of the time-dependent Navier–Stokes equations together with a verification obtained from the steady-state equations has also been obtained using numerical methods by Badr, Dennis & Young (1989) for the same Reynolds numbers and for $0 \leqslant \alpha \leqslant 1$. The flow in these cases tends to a steady pattern generally consistent with those of Loc (1975) and Ingham (1983) but there are differences in the lift and drag coefficients in all three studies. For these small Reynolds numbers there is no vortex detachment at any stage of the unsteady flow.

Unsteady flow past a rotating cylinder has previously been investigated experimentally by Coutanceau & Ménard (1985) for $R = 200$ and $0.5 \leqslant \alpha \leqslant 3.25$. Badr & Dennis (1985) gave numerical solutions of the full Navier–Stokes equations for small rotation rates $\alpha = 0.5$, 1.0 and $R = 200$ and 500, in which comparisons with Coutanceau & Ménard's experiments at $R = 200$ were given. Further comparisons of the experimental and calculated flow patterns at $R = 500$ and $\alpha = 0.5$, 1.0 were given

in a note by Badr *et al.* (1985). The range of R considered in the present work is $10^3 \leqslant R \leqslant 10^4$, while α ranges between 0.5 and 3. Numerous new effects appear when the Reynolds number is as high as 10^3 or above and a careful correlation of calculated and experimental results is presented over the complete range of α. The periodic nature of the flow field for small values of α is visualized in the calculations, indicating periodicity of even the very fine details of evolution of the wake. The similarities and differences between the present calculations at high R and those calculated by Ece *et al.* (1984) from boundary-layer theory are noted.

2. Theoretical and experimental summary

For a cylinder of radius a which starts its motion impulsively from rest with a linear velocity U and an angular velocity ω_0 in a fluid of kinematic viscosity ν, the two basic flow parameters are the Reynolds number $R = 2aU/\nu$ and the velocity ratio $\alpha = a\omega_0/U$. Polar coordinates (r, θ) are taken with the origin at the centre of the cylinder. The translational motion of the cylinder is in the direction $\theta = \pi$ while the rotational motion is counterclockwise. The unsteady Navier–Stokes equations in terms of the variables (ξ, θ), where $\xi = \ln(r/a)$, are given by Badr & Dennis (1985) in the form

$$e^{2\xi}\frac{\partial\zeta}{\partial\tau} = \frac{2}{R}\left(\frac{\partial^2\zeta}{\partial\xi^2}+\frac{\partial^2\zeta}{\partial\theta^2}\right)-\frac{\partial\psi}{\partial\theta}\frac{\partial\zeta}{\partial\xi}+\frac{\partial\psi}{\partial\xi}\frac{\partial\zeta}{\partial\theta}, \tag{1}$$

$$\frac{\partial^2\psi}{\partial\xi^2}+\frac{\partial^2\psi}{\partial\theta^2} = e^{2\xi}\zeta, \tag{2}$$

where ψ is the stream function and ζ is the (negative) scalar vorticity. These quantities are all dimensionless and are defined in Badr & Dennis (1985). The boundary conditions are based on the no-slip and impermeability conditions on the cylinder surface and the free-stream conditions away from it. These conditions can be expressed as

$$\psi = 0, \quad \frac{\partial\psi}{\partial\xi} = -\alpha \quad \text{at} \quad \xi = 0, \tag{3a}$$

and

$$e^{-\xi}\frac{\partial\psi}{\partial\theta} \to \cos\theta, \quad e^{-\xi}\frac{\partial\psi}{\partial\xi} \to \sin\theta \quad \text{as} \quad \xi \to \infty. \tag{3b}$$

Badr & Dennis (1985) have developed a method of solution of (1) and (2) by means of the substitutions

$$\psi(\xi,\theta,\tau) = \tfrac{1}{2}F_0(\xi,\tau)+\sum_{n=1}^{\infty}[F_n(\xi,\tau)\cos n\theta + f_n(\xi,\tau)\sin n\theta], \tag{4a}$$

$$\zeta(\xi,\theta,\tau) = \tfrac{1}{2}G_0(\xi,\tau)+\sum_{n=1}^{\infty}[G_n(\xi,\tau)\cos n\theta + g_n(\xi,\tau)\sin n\theta], \tag{4b}$$

which are a generalization of those used by Collins & Dennis (1973) in the case of the symmetrical flow generated when $\alpha = 0$. The equations and boundary conditions satisfied by the various functions appearing in the series (4) are given by Badr & Dennis, together with the method of solution, which makes use of the boundary-layer structure, but without any approximations to the Navier–Stokes equations. The only other point worth emphasizing is that the boundary conditions on the functions $F_n(\xi,\tau)$ and $f_n(\xi,\tau)$ corresponding to (3) are utilized to deduce sets of global

conditions, termed integral conditions (see Dennis & Quartapelle (1989) for further explanation of these conditions), on the functions $G_n(\xi,\tau)$ and $g_n(\xi,\tau)$. These are employed in the solution procedure to ensure that all necessary conditions of the problem are satisfied. For example, Badr & Dennis (1985) have shown that the condition

$$\int_0^\infty \mathrm{e}^{2\xi} G_0(\xi,\tau)\,\mathrm{d}\xi = 2\alpha, \tag{5}$$

which expresses the fact that the circulation round a contour at infinite distance from the cylinder and concentric with it remains zero with time, must be satisfied in order for the pressure on the cylinder surface to remain single-valued. It is easily shown that (5) does enforce zero circulation round an infinitely large contour surrounding the cylinder by integrating once in the ξ-direction the equation for $G_0(\xi,\tau)$ obtained by substitution of (4*a*, *b*) in (2) and employment of the result

$$\Gamma(\xi,\tau) = -\pi\left(\frac{\partial F_0}{\partial \xi}\right)_{\xi=\xi_0} \tag{6}$$

for the circulation $\Gamma(\xi,\tau)$ round a circular contour $\xi = \xi_0$. Sets of integral conditions on $G_n(\xi,\tau)$, $g_n(\xi,\tau)$ for $n \neq 0$ ensure that the correct external flow conditions are satisfied.

The solution procedure using boundary-layer coordinates has been described by Badr & Dennis (1985). The grid size Δz in the coordinate z, defined by $\xi = 2(2\tau/R)^{\frac{1}{2}} z$, is more or less independent of R. The value $\Delta z = 0.05$ was taken for the Reynolds numbers $R = 10^3$ and 10^4 considered here. The maximum value of the computational field length was $z_M = 8$ and the maximum number of terms used in the series (4*a*, *b*) corresponds to replacing the infinite upper limit in each sum by the finite integer $N = 20$. The discussion of the choice of these various parameters is in principle the same as that given by Badr & Dennis (1985, pp. 459–460) and the time steps $\Delta\tau$ used for the evolution of the solution follow exactly those set out in that discussion.

In the corresponding experimental study, the set-up is in principle the same as that used by Coutanceau & Bouard (1977) and Bouard & Coutanceau (1980) to study the evolution of the wake in the case of no rotation ($\alpha = 0$), but with various modifications described by Ménard (1984). The cylinder moves vertically upwards in a large tank filled with water. The rotational motion is linked mechanically to the translational one and the cylinder starts translating and rotating simultaneously from rest. However, because of inertia effects, the actual start of the motion is quasi-instantaneous and the limiting steady translational and rotational speeds are reached after a few hundredths of a second. Nevertheless, this is a good approximation to the theoretical impulsive start of the motion.

Two cylinders, of diameters 4 cm and 6 cm, were used. The liquid tank has dimensions of 46×56 cm in cross-section and 1 m height. The cylinder moves midway between the tank walls to minimize the wall effects, while the clearance between the ends of the cylinder and the tank walls is as small as possible to reduce end effects. The flow is visualized using small, brightly illuminated, solid plastic tracer particles of Rilson powder which are photographed at given selected times by a camera translating with the cylinder. Essential details of the whole procedure are given by Coutanceau & Ménard (1985, pp. 402–405).

3. Calculated and experimental results and comparisons

In this section, we present a comparative study of both the calculated and experimental evolution of the flow field for $R = 10^3$ and $0.5 \leqslant \alpha \leqslant 3$. At low rotational rates $\alpha = 0.5, 1.0$, the general nature of the time development of the flow is similar to that at corresponding values of α for $R = 200$ and 500 reported by Coutanceau & Ménard (1985) and Badr & Dennis (1985), especially with regard to the formation and shedding of the large vortices. However, on the microscale the flow at $R = 10^3$ is different since many secondary vortices are formed adjacent to the large ones. Because of limitations of the experimental apparatus, it is only possible to observe the formation of the first few vortices for any value of R and α and their detachment into the wake of the cylinder. Accordingly, comparisons between theoretical and experimental results are carried out up to the time of termination of the experiment. However, the numerical solutions were continued to larger times.

We first consider the details of the case $R = 10^3$, $\alpha = 0.5$. Immediately after the impulsive start of the motion, the stagnation point T_1 which would be at the rear of the cylinder in the case of zero rotation ($\alpha = 0$) follows the direction of rotation round to an instream position (located by the condition $\partial\psi/\partial\xi = \partial\psi/\partial\theta = 0$) at about $\theta = 135°$, $r/a = 1.04$ where it starts to stabilize. Its subsequent location can be seen in figure 1, which shows the instantaneous streamline patterns adjacent to the cylinder for $\tau = 1$ to 16. The birth of the first eddy E_1 with closure point S_1 occurs at $\tau = 1$ in an instream position of the region $0 \leqslant \theta \leqslant 90°$ (figure 1*a*). A discussion of the formation of such an eddy has been given by Badr & Dennis (1987). The eddy E_1 is followed almost immediately by the formation of the second eddy E_2 in the region $270° \leqslant \theta \leqslant 360°$ (see figure 1*b*). At $\tau = 3$, a secondary eddy E_1' appears in the region $0 \leqslant \theta \leqslant 90°$ and is seen in both figures 1(*c*) and 1(*c'*). This phenomenon is similar to that observed by Bouard & Coutanceau (1980) in the case of $\alpha = 0$. At the same time $\tau = 3$ a secondary eddy E_2' also appears near the cylinder in the neighbourhood of E_2. The elongation of E_2' in the direction of the cylinder rotation tends to form a tongue of fluid which at $\tau = 4$ gives rise to a new secondary eddy denoted by E_2'' in figures 1(*d*) and 1(*d'*). Thus the main vortex E_2 is now accompanied by two small eddies E_2' and E_2''.

At about $\tau = 6$ (figure 1*e*), the size of E_1 reaches its maximum while it starts moving in the downstream direction. On the other hand the secondary vortices E_1' and E_2'' have disappeared while E_2' is vanishing. At $\tau = 8$, the main vortex E_1 is shed away from the cylinder and phenomena analogous to the ones observed by Coutanceau & Ménard (1985), Badr & Dennis (1985) for $R = 200$ and 500 appear. Thus E_3' is formed upstream of E_1, i.e. here in place of E_1', while at the same time E_2 has been considerably elongated along the direction of the cylinder rotation and a new eddy E_3'' is well formed in the fluid corner between E_2 and the surface of the cylinder, i.e. here in place of E_2'; but, for this high value of R, the eddy E_3'' is again accompanied by a secondary eddy E_3'''. This situation is indicated in figure 1(*f*).

We note that in the analysis of both theoretical and experimental results special care has been taken to determine the location of the centres of vortices as well as their closure points. Both are determined by the conditions $\partial\psi/\partial\xi = \partial\psi/\partial\theta = 0$. These special points play a crucial role in determining the nature of the flow and the mechanics of vortex detachment and shedding as described in detail by Badr *et al.* (1986) and Badr & Dennis (1987). The movement of the closure point of E_2 (denoted by S_2) is remarkable between $\tau = 6$ and $\tau = 8$.

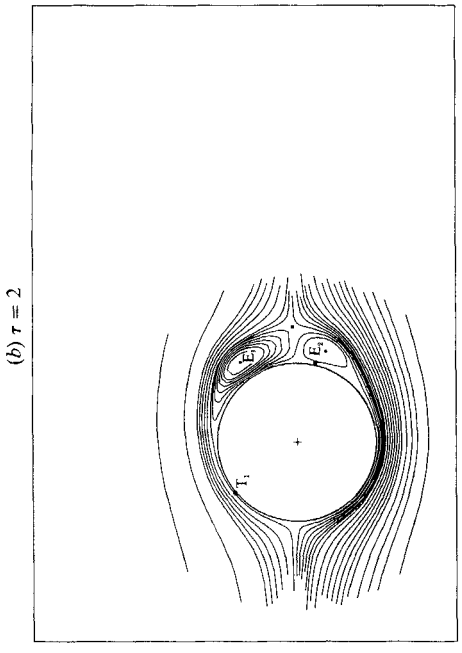
(b) τ = 2
E'1
E1
T1

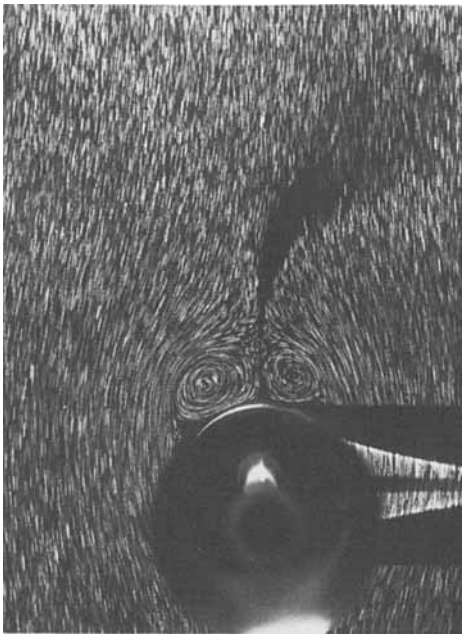
(c') τ = 3

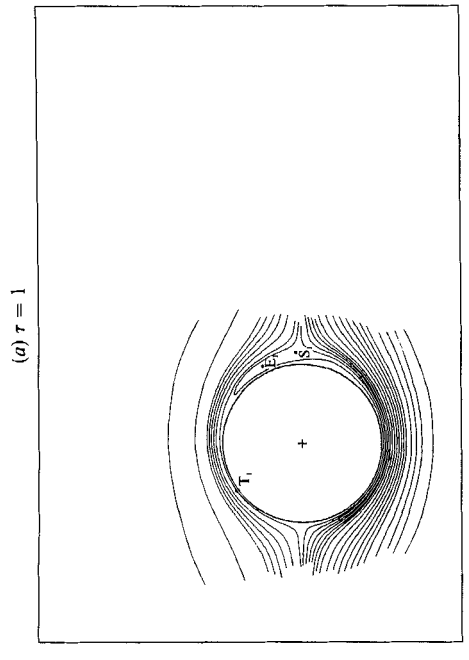
(a) τ = 1
E'2
S'
T1

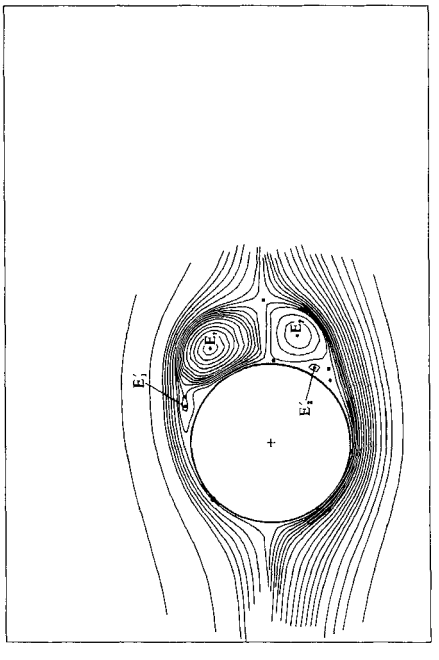
(c) τ = 3
E'2
E'1
E'3
E1
Φ

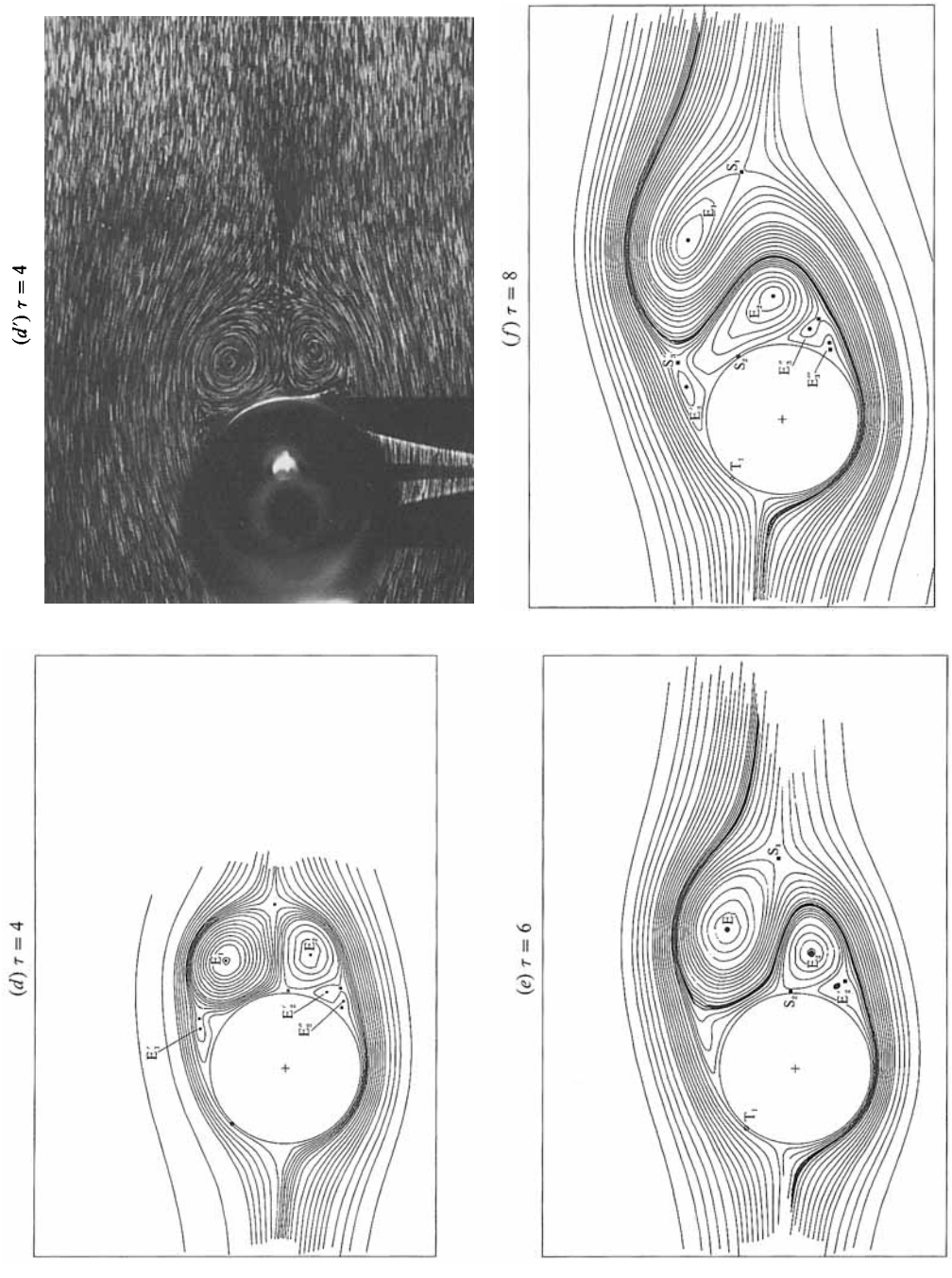

FIGURE 1 (*a–f*). For caption see next page.

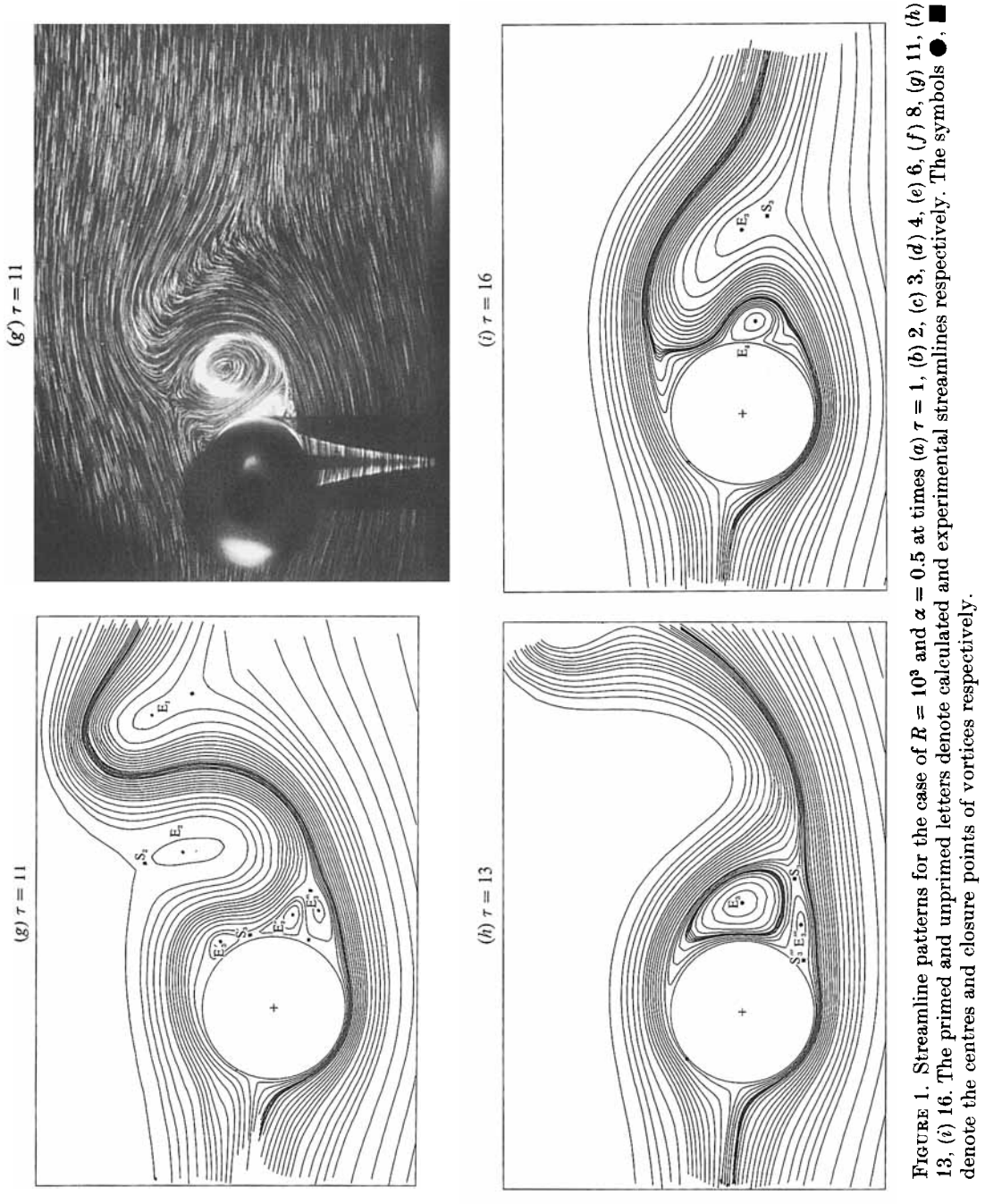

FIGURE 1. Streamline patterns for the case of $R = 10^3$ and $\alpha = 0.5$ at times (*a*) $\tau = 1$, (*b*) 2, (*c*) 3, (*d*) 4, (*e*) 6, (*f*) 8, (*g*) 11, (*h*) 13, (*i*) 16. The primed and unprimed letters denote calculated and experimental streamlines respectively. The symbols ●, ■ denote the centres and closure points of vortices respectively.

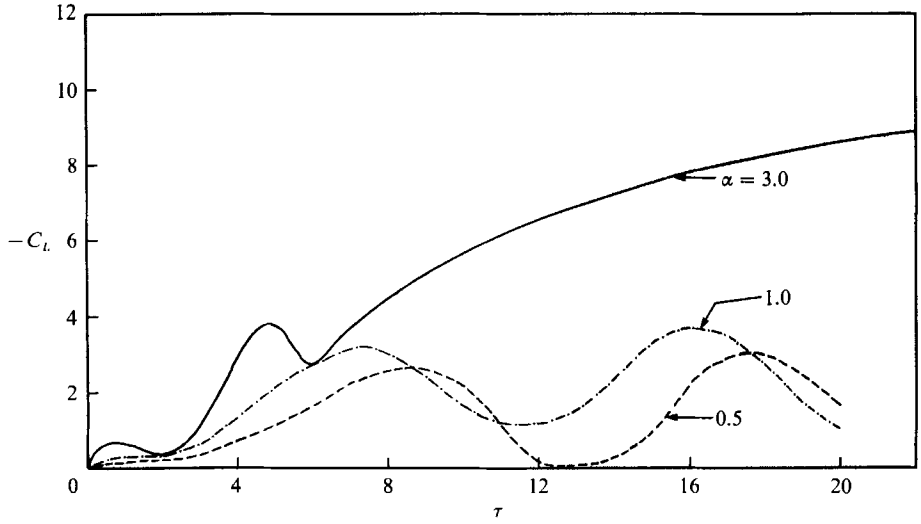

FIGURE 2. The time variation of the lift coefficient C_L for $R = 10^3$ and $\alpha = 0.5$, 1.0 and 3.0.

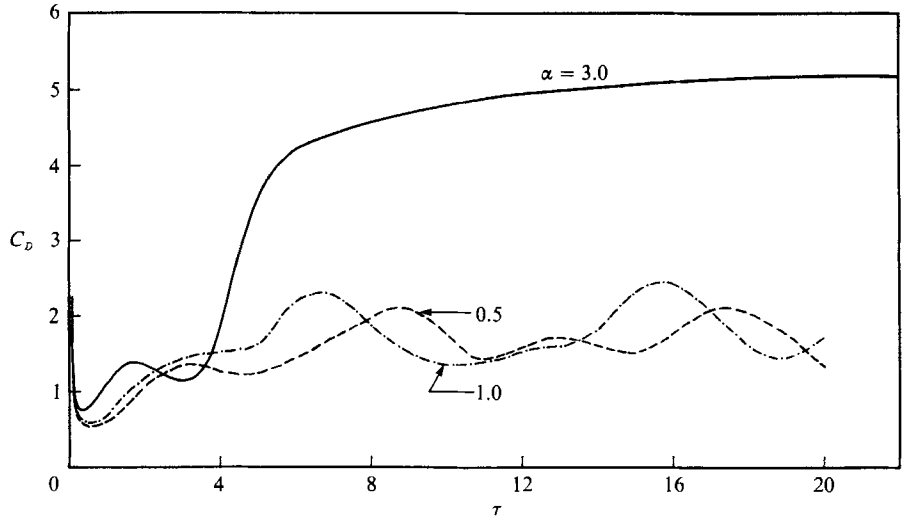

FIGURE 3. The time variation of the drag coefficient C_D for $R = 10^3$ and $\alpha = 0.5$, 1.0 and 3.0.

At $\tau = 11$, (figures 1*g*, 1*g'*), E_2 is detached owing to a transposition of its closure point with the one of E_3'. Simultaneously there is an analogous transposition between the closure points of E_3'' and E_3''' respectively, so that E_3'' is now turned towards E_3' and E_3''' towards downstream. Progressively E_3' and E_3'', which have the same direction of rotation, approach each other until their closure points come into contact to form a common one. The two vortices are about to coalesce; details of such a coalescence have been described by Coutanceau & Ménard (1985) and numerically by Badr & Dennis (1987). At $\tau = 13$ (figure 1*h*), the coalescence of E_3' and E_3'' is effective and the corresponding vortex E_3 is detaching owing to the transposition of its closure point with that of E_3''' which is again turned towards the cylinder surface. In its turn, E_3''' is elongated along the rotating cylinder and gives rise to what it is logical to call E_4

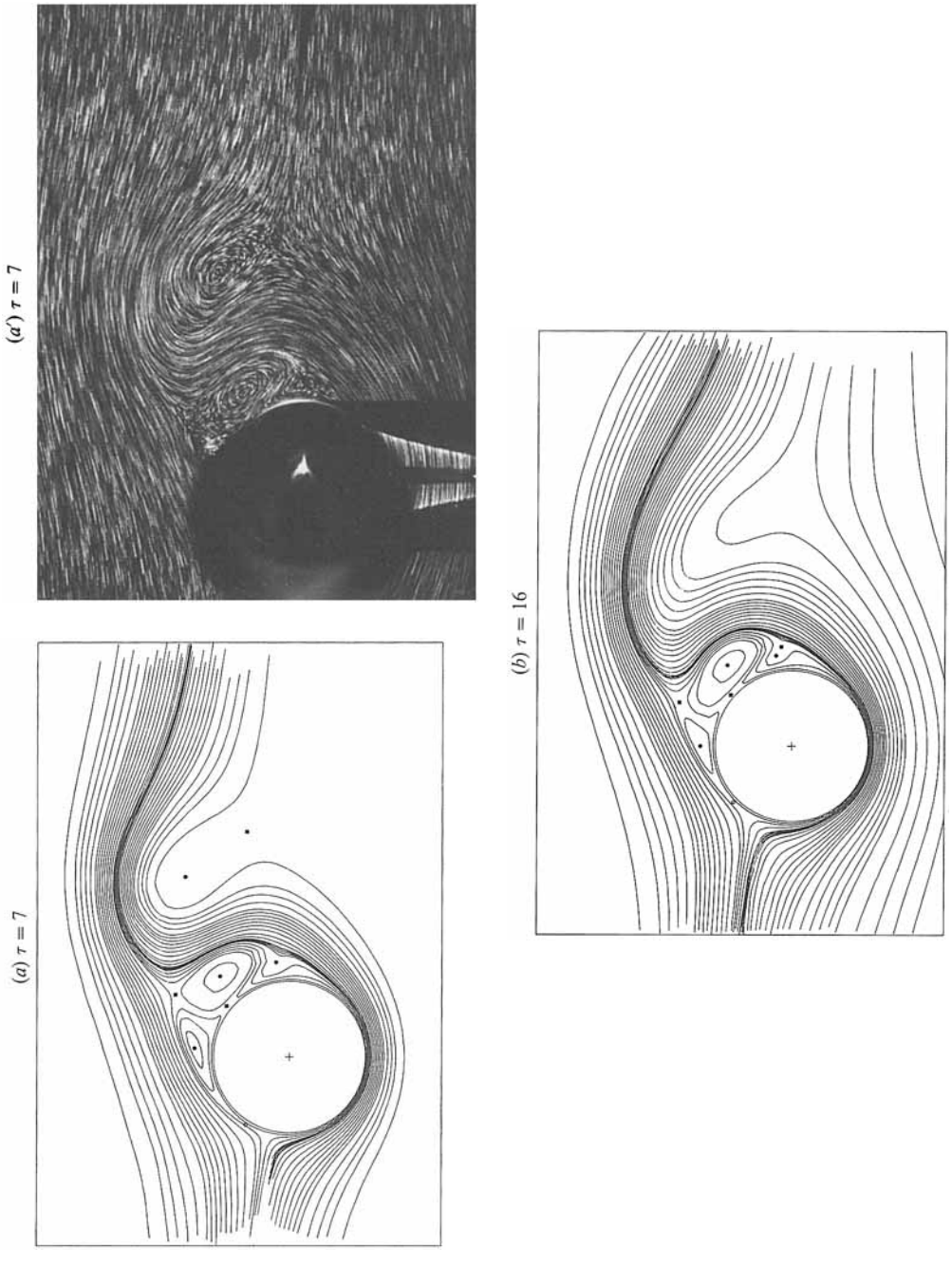

FIGURE 4. Comparison between the streamline patterns for $R = 10^3$ and $\alpha = 1$ at times (*a*) $\tau = 7$ and (*b*) $\tau = 16$ showing the periodicity of the flow field. The notation for primed and unprimed letters follows figure 1.

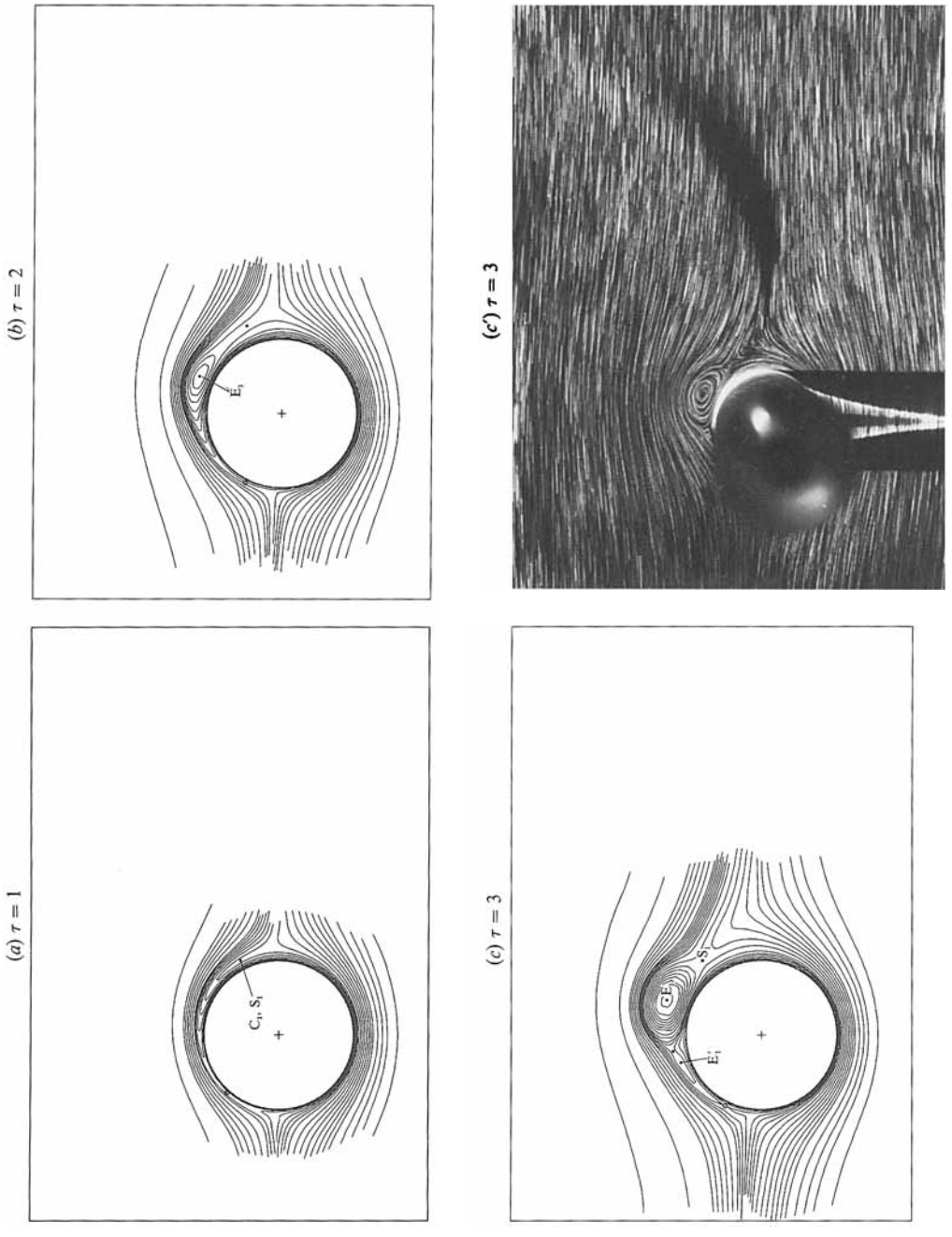

FIGURE 5 (*a–c'*). For caption see page 472.

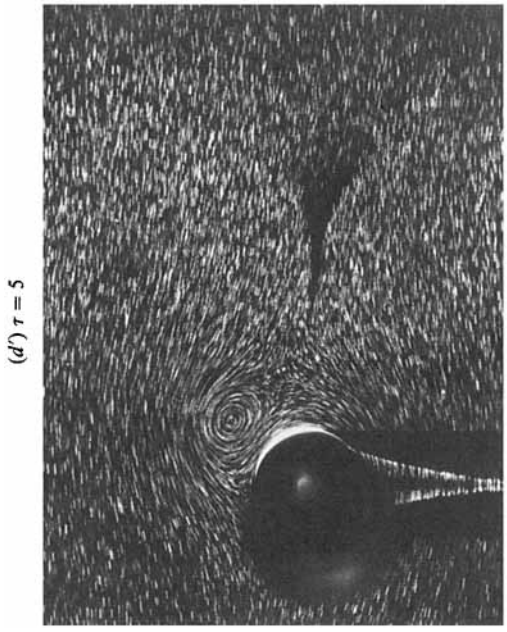

(d') $\tau = 5$

(e') $\tau = 9$

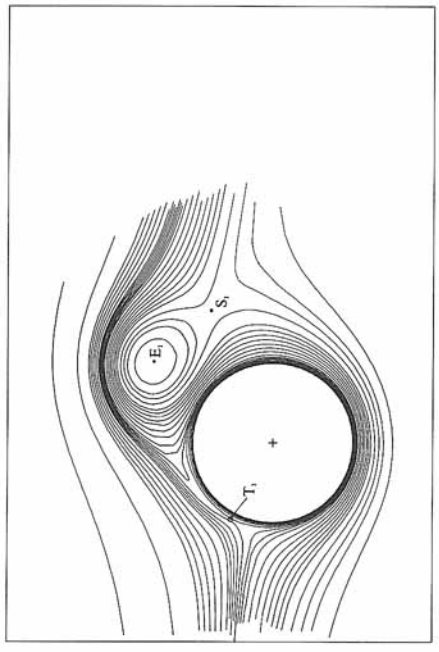

(d) $\tau = 5$

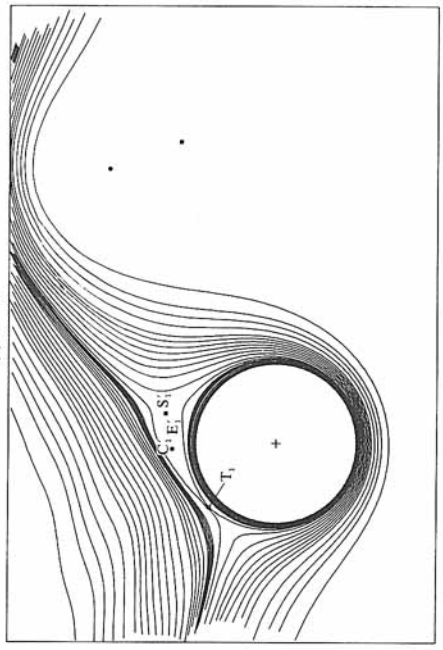

(e) $\tau = 9$

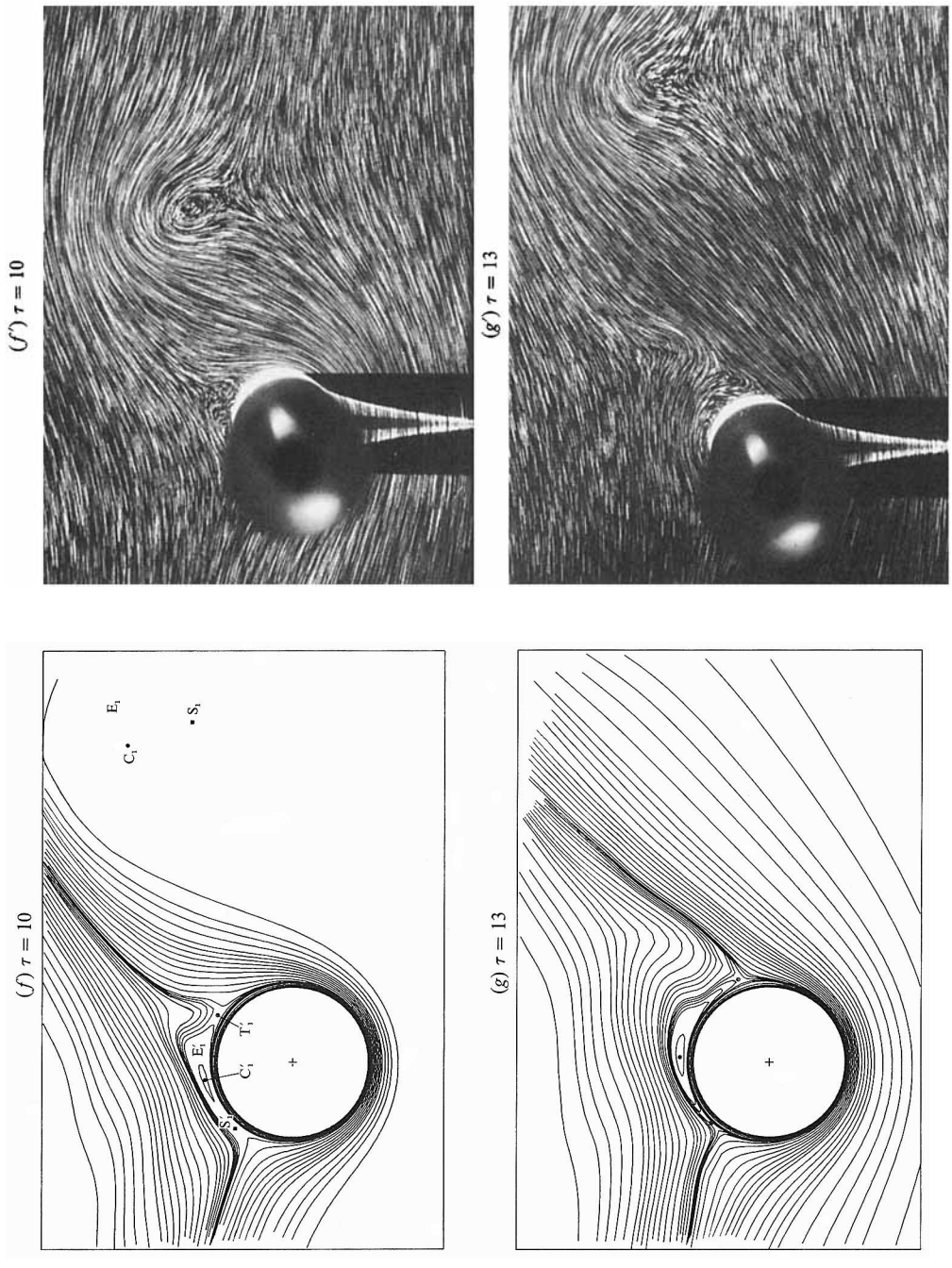

FIGURE 5(*d*–*g*′). For caption see next page.

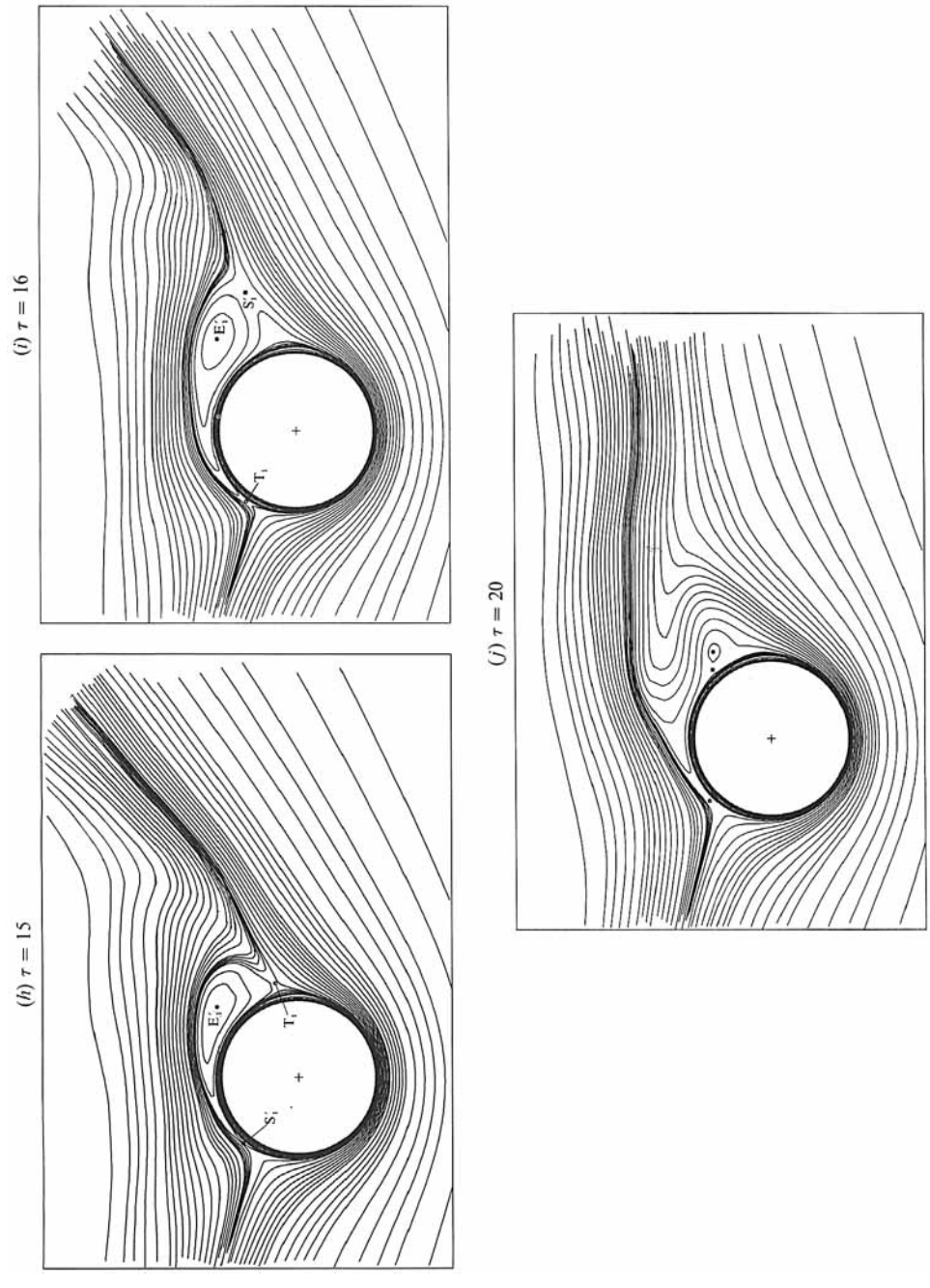

FIGURE 5. The experimental and theoretical flow patterns for $R = 10^3$ and $\alpha = 2$ at times (*a*) $\tau = 1$, (*b*) $\tau = 2$, (*c*) $\tau = 3$, (*d*) $\tau = 5$, (*e*) $\tau = 9$, (*f*) $\tau = 10$, (*g*) $\tau = 13$, (*h*) $\tau = 15$, (*i*) $\tau = 16$, (*j*) $\tau = 20$. The notation for primed and unprimed letters and the centres and closure points of vortices follows figure 1.

because it will be shed just after E_3. At time $\tau = 16$, (figure 1*i*), the vortex E_3 is effectively shed away from the cylinder and E_4 starts growing in a similar way to the growth of E_2 at $\tau = 7$. So the process continues but the vortices are somewhat weaker.

In figure 2 we show the variation of the calculated lift coefficient C_L with τ for the case of $R = 10^3$ and the three rotation rates of $\alpha = 0.5$, 1.0 and 3.0; figure 3 gives the corresponding variation of C_D. For the lower rotation rates, a periodic variation associated with vortex shedding soon develops and continues indefinitely. For $\alpha = 0.5$ the period of about $\tau = 9$ is completely consistent with the start, at $\tau = 16$, of the repetition of the sequence of phenomena which first start at $\tau = 7$, and which have just been described. We can perform a check on the periodicity of the structure of the flow by comparing the streamline patterns at times approximately one complete period apart. For $\alpha = 1.0$ we find from figures 2 and 3 that the period is again approximately 9.0. In figure 4 the streamline patterns found from the calculations for $\alpha = 1$ at $\tau = 7$ and at $\tau = 16$ are shown, together with the experimental visualization at $\tau = 7$. They confirm to reasonably good precision the periodicity of the flow field and the excellent measure of agreement with the experiments at $\tau = 7$.

In figure 5, the calculated evolution of the flow field for $\alpha = 2$ is given, together with the experimental flow visualization between $\tau = 1$ and 15. At $\tau = 1$ (figure 5*a*) the first vortex appears where the centre C_1 and closure point S_1 coincide. Badr & Dennis (1987) describe generally this process. As τ increases, E_1 grows and is swept in the direction of the cylinder rotation while there is no indication of the formation of a second vortex. At $\tau = 3$ (figures 5*c*, 5*c*′), a secondary vortex E_1' is formed adjacent to E_1 similar to the one formed for $\alpha = 0.5$, but clearly more toward the front of the cylinder. At $\tau = 5$ (figure 5*d*, 5*d*′), E_1' disappears while E_1 has moved away from the cylinder. The motion of E_1 away into the wake continues with no more vortex formation until $\tau = 9$ (figures 5*e*, 5*e*′), when a new clockwise vortex E_1' forms at the top of the cylinder. The growth of E_1' with time continues until $\tau = 15$. Between $\tau = 15$ and 16, the closure point of E_1' moves quickly in the downstream direction signalling the beginning of its shedding. At $\tau = 20$ the calculations (which, contrary to the experiments, have been continued until this time) show that a small counterclockwise vortex forms very late, initiating probably the alternate vortex shedding process but with extremely weak counterclockwise vortices. However, it is quite clear that the increase of α tends to suppress the process of vortex formation behind the cylinder. This trend is shown both theoretically and experimentally throughout figure 5.

Another equally interesting phenomenon occurs in the case of $\alpha = 2$; two successive transpositions take place between the closure point of E_1' and the front stagnation point T_1. At $\tau = 9$, the eddy E_1' has its closure point S_1' downstream and the front stagnation point T_1 upstream. This is followed immediately by the transposition of S_1' and T_1 as can be seen at $\tau = 10$. This orientation of S_1' and T_1 continues until approximately $\tau = 16$ when T_1 and S_1' change positions again and soon after E_1' starts shedding downstream away from the cylinder surface. The excellent comparison between the experimental and theoretical flow patterns shown in figure 5 tends to confirm the degree of accuracy of both numerical and experimental methods used in this study.

In the case of $\alpha = 3$, a periodic flow pattern does not develop with time as is evident from figures 2 and 3. At this speed of rotation, no eddies are formed up to $\tau = 1$ unlike the behaviour when $\alpha \leqslant 2$ (see figure 6*a*). At $\tau = 2$ (figure 6*b*), an eddy

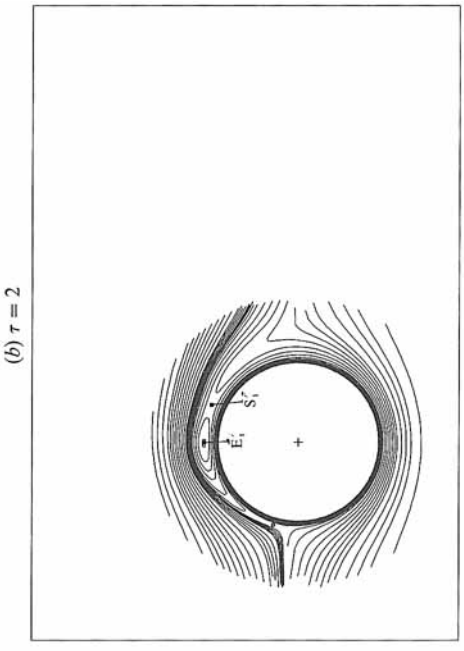
(b) τ = 2
S'1
E'1

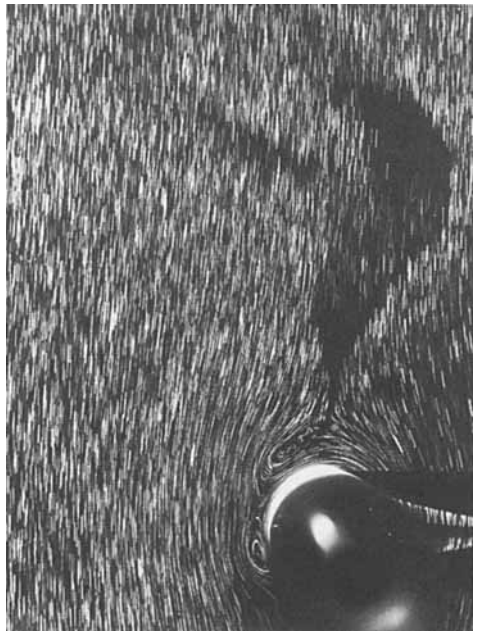
(c') τ = 3

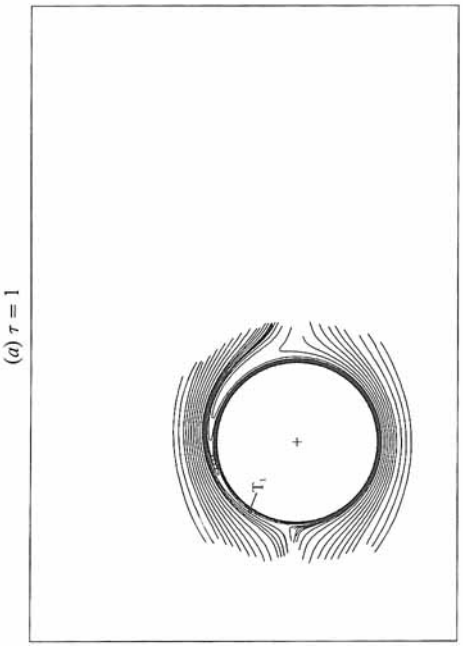
(a) τ = 1
T1

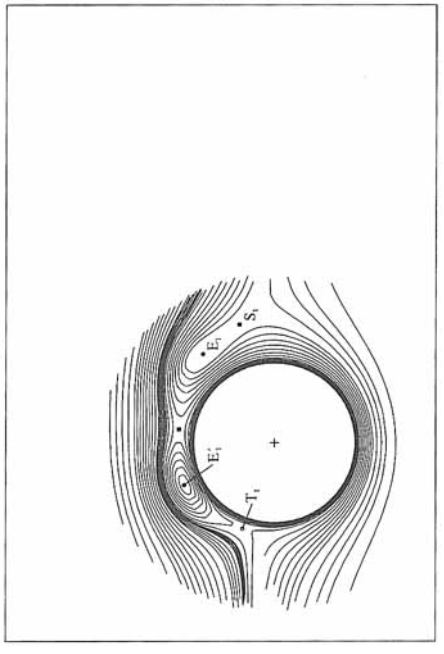
(c) τ = 3
S1
E'1
E1
T1

(*d'*) $\tau = 4$

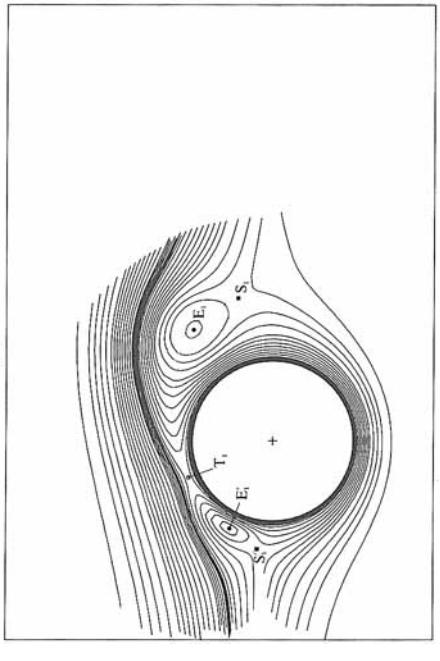

(*d*) $\tau = 4$

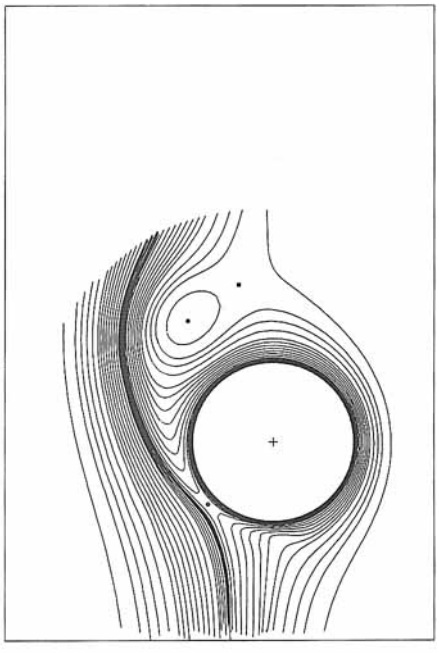

(*f*) $\tau = 4.4$

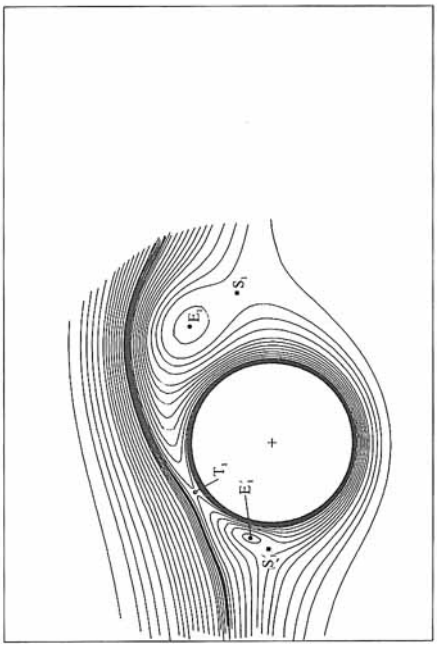

(*e*) $\tau = 4.2$

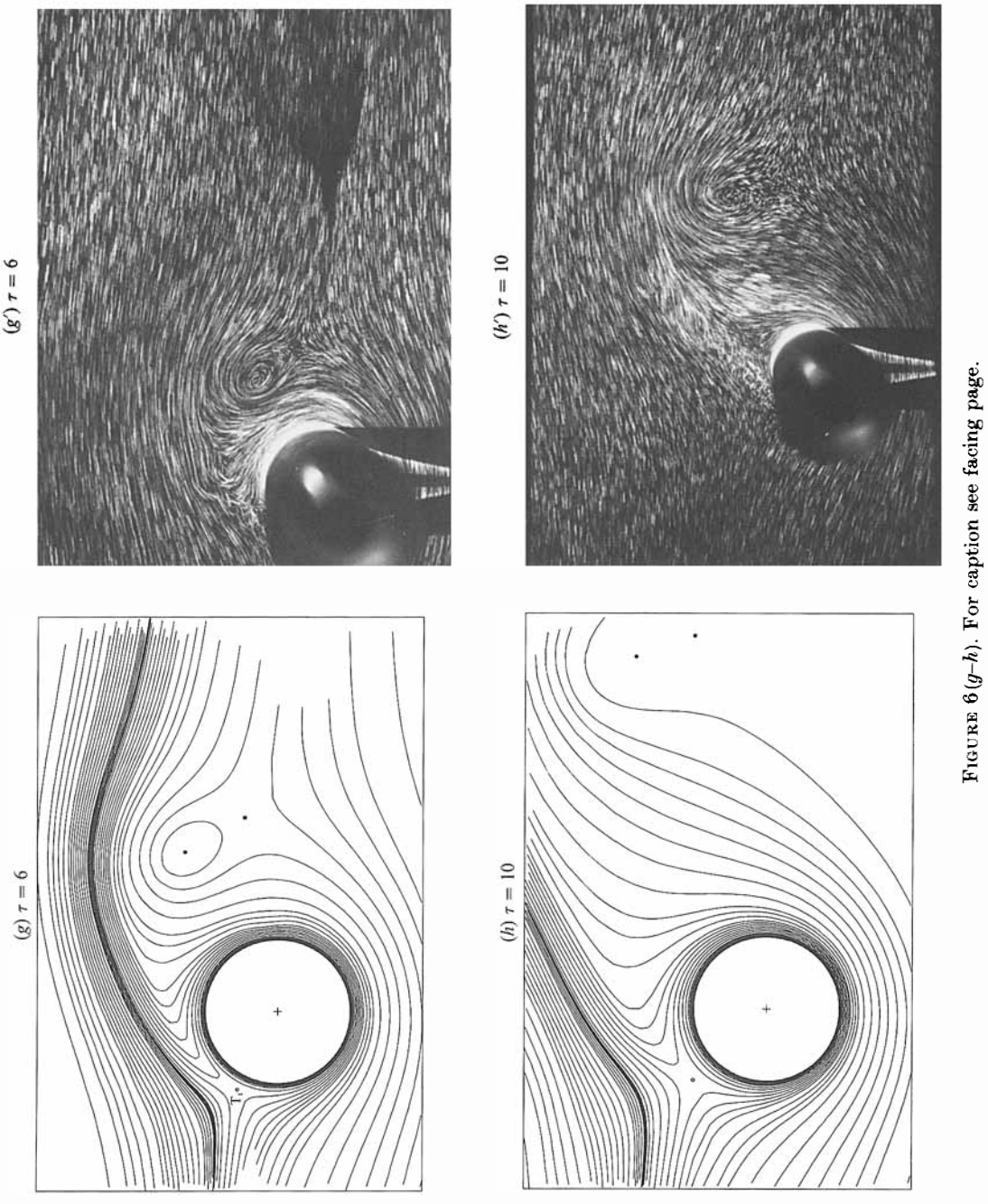

FIGURE 6 (*g–h*). For caption see facing page.

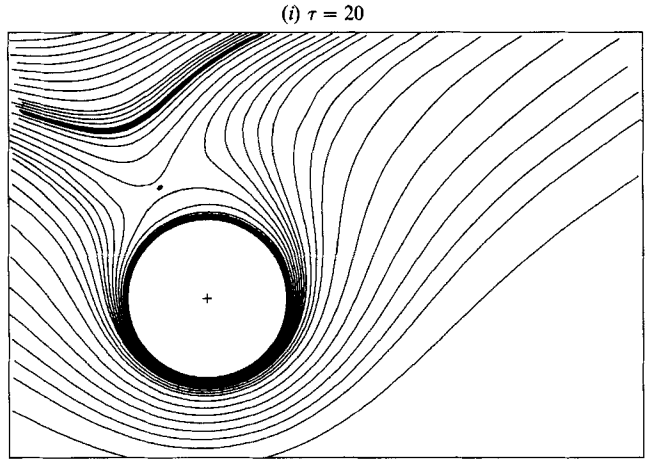

FIGURE 6. The experimental and theoretical flow patterns for $R = 10^3$ and $\alpha = 3$ at times (*a*) $\tau = 1$, (*b*) $\tau = 2$, (*c*) $\tau = 3$, (*d*) $\tau = 4$, (*e*) $\tau = 4.2$, (*f*) $\tau = 4.4$, (*g*) $\tau = 6$, (*h*) $\tau = 10$, (*i*) $\tau = 20$. The notation for primed and unprimed letters and the vortex centres and closure points follows figure 1.

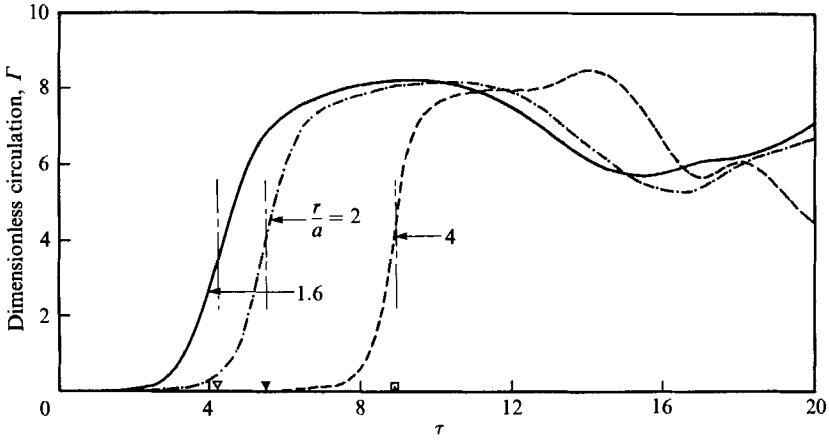

FIGURE 7. The time variation of the circulation Γ around the circular contours $r/a = 1.6$, 2 and 4 for the case of $R = 10^3$, $\alpha = 2$. The symbols ▽, ▼, ⊡ show the time at which the centre of the first vortex crosses these boundaries respectively.

E_1' is formed at the top of the cylinder and soon after (at $\tau = 3$) another eddy E_1 is formed in the first quadrant. The two eddies, which have the same sense of rotation, start moving in different directions, as can be seen experimentally and theoretically at $\tau = 4$ (figures 6*d*, 6*d'*) and theoretically at $\tau = 4.2$ (figure 6*e*), owing to the transposition of T_1 and S_1'. While E_1' is influenced by the high speed of the cylinder surface, E_1 is more influenced by the main stream. Soon after $\tau = 4.2$, at $\tau = 4.4$ (figure 6*f*), E_1' is washed down to the frontal part of the cylinder and disappears, while E_1 continues shedding downstream. This is followed by no more formation of any eddies and the flow field possesses only one stagnation point T_1 as can be seen in figure 6(*g*, *h*). As the time increases, the calculated flow field approaches a steady state (figure 6*h*, *i*). Comparison with the experiments is excellent until reaching $\tau = 6$; however, the experimental technique did not visualize the region upstream of

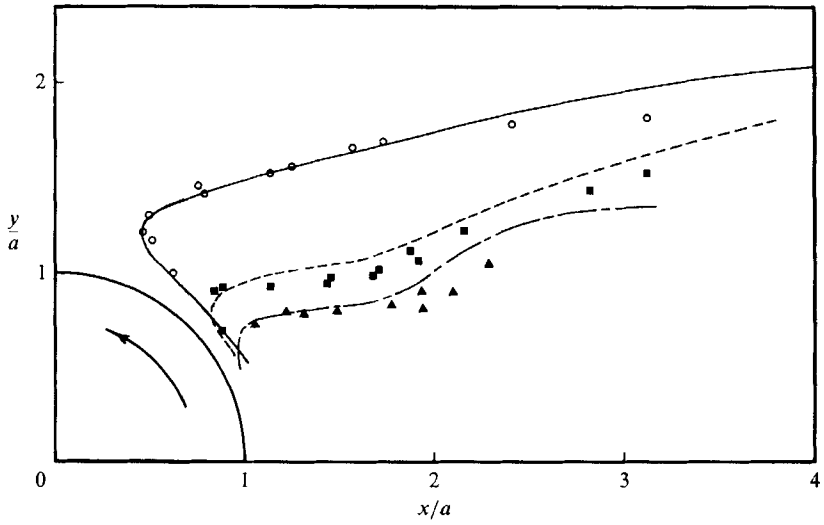

FIGURE 8. Comparison between the paths of the first vortex obtained theoretically and experimentally for $R = 10^3$ and $\alpha = 0.5$, 1.0 and 2.0. Calculated results: ——, $\alpha = 0.5$; – – – –, $\alpha = 1$; ——, $\alpha = 2$. Experimental points: ▲, $\alpha = 0.5$; ■, $\alpha = 1.0$; ○, $\alpha = 2.0$.

the cylinder in this case, but analogous situations were visualized for $R = 200$ and $\alpha = 2.07$ and 3 given by Coutanceau & Ménard (1985). Moreover, following $\tau = 6$, three-dimensional and instability effects become more pronounced, especially in the wake, and therefore no further sensible comparisons can be made.

The time variation of the dimensionless circulation Γ round a fixed circular contour is also investigated. Figure 7 shows the variation of Γ with time for the case of $R = 10^3$, $\alpha = 2$ at the three contours defined by $r/a = 1.6$, 2 and 4. The time at which the first vortex centre C_1 crosses these contours is also labelled in the figure. It is clear that the first sharp rise of Γ at the three contours occurs when the centre of E_1 crosses each of them. Subsequent changes of Γ occur because of the shedding of the eddies which follow later.

To provide some quantitative comparison between the theoretical and experimental results, the path of the first vortex centre C_1 for each of the three cases $\alpha = 0.5$, 1.0 and 2.0 is plotted in figure 8. In this figure we can discern the effect of the blockage ratio of the experiments, which invariably causes the vortices to be deflected towards the axis aft of the cylinder after they have detached into the wake and more so as they move farther from the cylinder. The experimental points in figure 8 were obtained with the 4 cm diameter cylinder, giving the smaller blockage ratio. For the 6 cm diameter cylinder (see Ménard 1984) the experimental points are generally displaced further towards the axis. Figure 9 (a, b, c) shows a comparison between the evolution of the velocity distribution at sections $\theta = 0$ and $\theta = 90°$ obtained both numerically and experimentally. A good comparison is found in all cases, with the exception of a small deviation of some of the experimental distributions of the x-component of the velocity on the axis $\theta = 0$ to the rear of the cylinder. However, since the velocity is small in this region such a deviation would be permissible in the analysis of the experimental results.

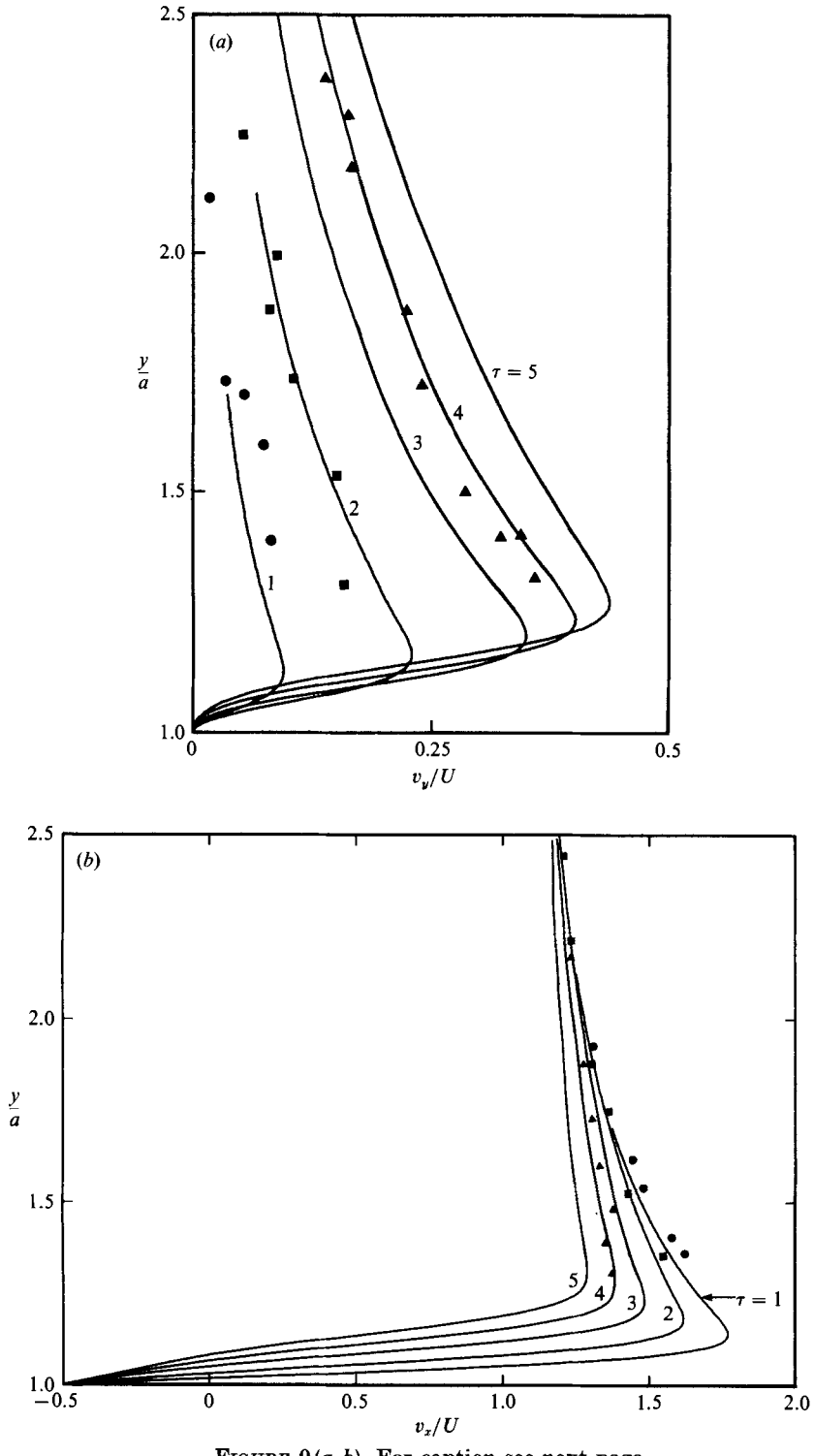

FIGURE 9(*a*, *b*). For caption see next page.

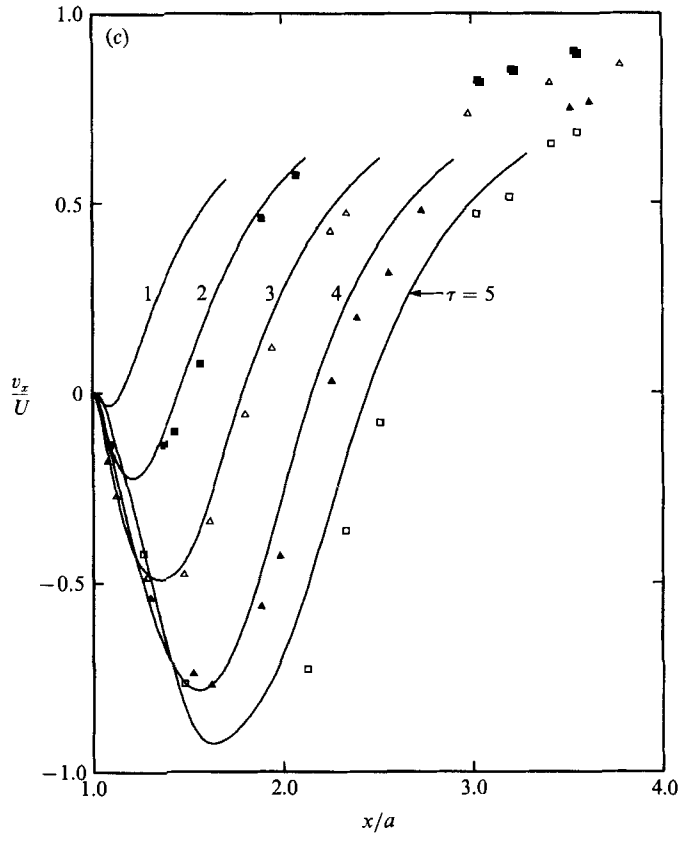

FIGURE 9. The evolution of the velocity distribution for the case of $R = 10^3$ and $\alpha = 0.5$; (*a*) v_y versus y at $\theta = 90°$, (*b*) v_x versus y at $\theta = 90°$, (*c*) v_x versus x at $\theta = 0$. Experimental points: ●, $\tau = 1$; ■, $\tau = 2$; △, $\tau = 3$; ▲, $\tau = 4$; □, $\tau = 5$.

4. Comparison of Navier–Stokes solutions with boundary-layer theory

As the Reynolds number becomes high, it is well known that boundary-layer theory can be applied to study the initial flow past impulsively started cylinders. The calculations of the present paper are based on the full Navier–Stokes equations without any boundary-layer approximations at any stage so it is of interest briefly to consider the case of large Reynolds number and its relationship with the boundary-layer limit of the equations of motion obtained by setting $R = \infty$. The solution of the boundary-layer equations was carried out by Ece *et al.* (1984). Here we consider the typical case of $R = 10^3$, $\alpha = 1$ and provide three solutions for the time variation of the lift coefficient. The first one is the small-time analytical solution given by Badr & Dennis (1985) and is based on the leading terms of the solution in powers of τ of the full Navier–Stokes equations, which yields

$$C_L = -1.4498\pi\alpha\lambda + \alpha\lambda\left[\frac{4}{3\pi^{\frac{1}{2}}} - 0.6961\pi\lambda\right], \tag{7}$$

where $\lambda = 2(2\tau/R)^{\frac{1}{2}}$ and the first term on the right-hand side represents the part of the lift coefficient due to the pressure forces C_{LP}, while the second term represents the contribution of the friction forces C_{LF}. The second estimate of C_L is based on the

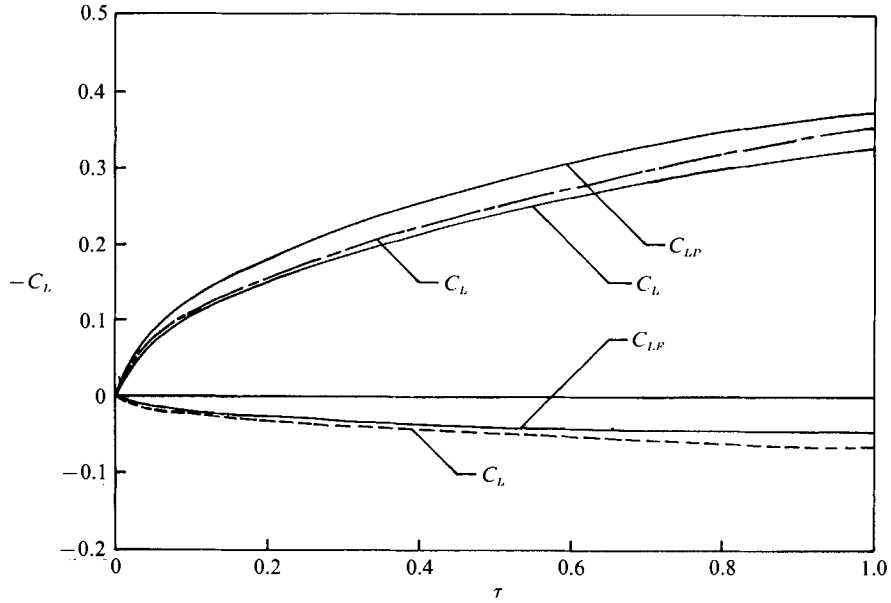

FIGURE 10. Comparison between the small-time variation of the lift coefficient obtained by solving the Navier–Stokes equations analytically and numerically and also by solving the boundary-layer limit of the equations for the case of $R = 10^3$, $\alpha = 1$: ——, numerical solution; – – – –, boundary-layer solution; — – —, analytical solution.

solution of the Navier–Stokes equations using the present numerical method. The third solution represents the small-time analytical solution of the boundary-layer limit ($R = \infty$) of the governing equations, which can be expressed as

$$R^{\frac{1}{2}}C_L = \alpha(128\tau/9\pi)^{\frac{1}{2}}. \tag{8}$$

The three solutions are plotted in figure 10 in the time range $\tau = 0$ to 1. It is clear from the figure that, while there is reasonable agreement between the numerical solution and the analytical approximation (7) to the Navier–Stokes equations, the boundary-layer limit of the equations of motion gives an erroneous value of C_L with a lift force acting in the wrong direction. This is explained by the fact that the lift coefficient given in (8) contains only the part of the lift resulting from the skin friction and with no contribution from pressure forces. Since the pressure forces much outweigh the friction forces in the present problem, the error is considerable. It is similarly found that the solution of the boundary-layer limit of the governing equations leads to a drag force which is not consistent with the high-Reynolds-number solution of the Navier–Stokes equations.

In order to compare the streamline patterns with the results given by Ece *et al.* (1984) for $R = \infty$, the case of high Reynolds number $R = 10^4$ is studied for $\alpha = 0.6$ in the time range $\tau = 0$ to 1.1. Ece *et al.* give exploded views of their computed streamline patterns for various rotation rates, since in the limiting case of $R = \infty$ the whole streamline pattern would occupy a space defined by the surface of the cylinder and having zero radial thickness. Figure 11 shows the time development of the flow field based on the numerical solution of the full governing equations for a typical case $\alpha = 0.6$. Although a quantitative comparison with Ece *et al.* is uncertain because they do not provide their exploded scale, the two flow fields are of a similar character qualitatively. The exploded views given in figure 11 are plotted by considering $r = e^z$

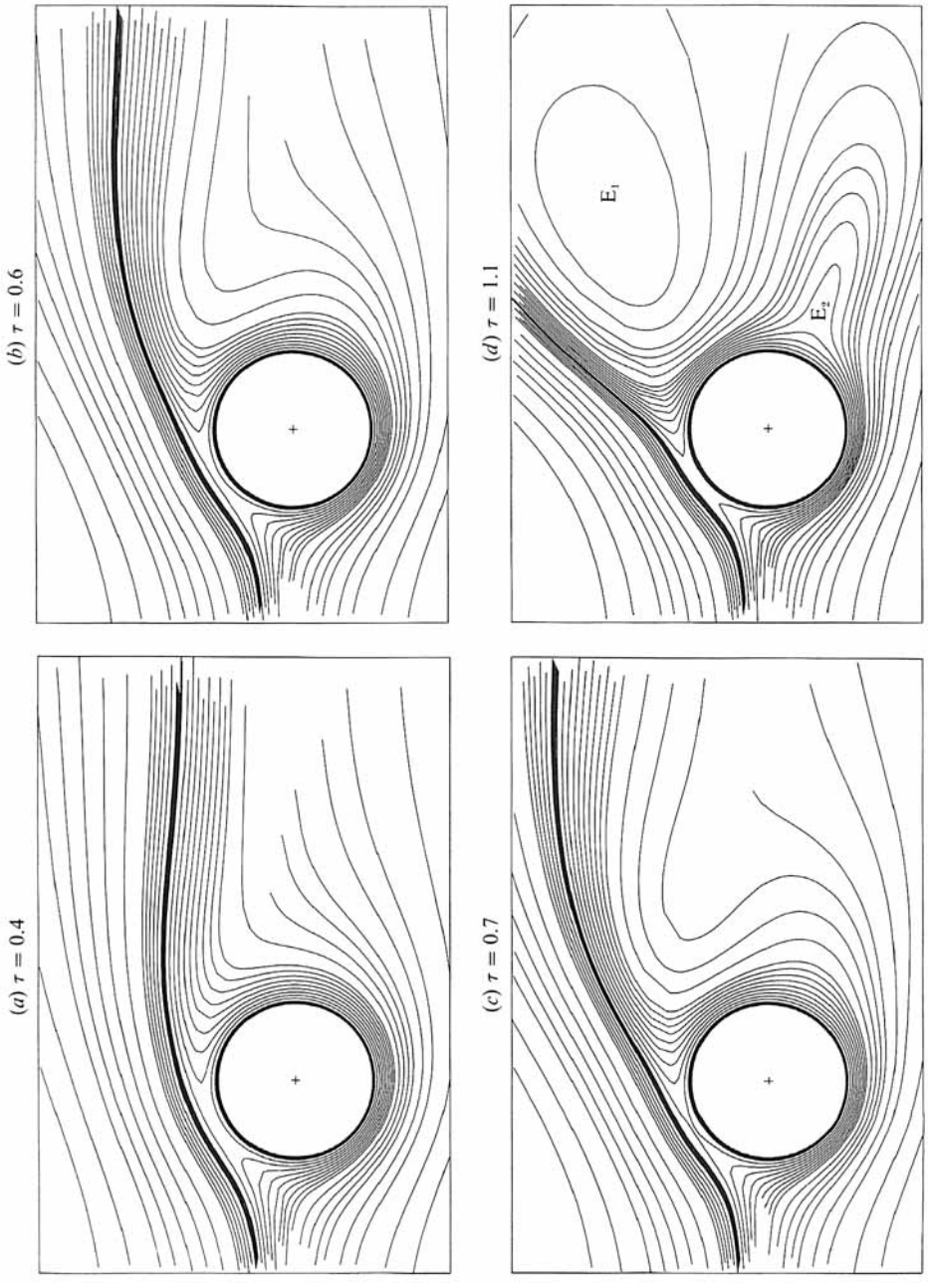

FIGURE 11. The streamline patterns for the case of $R = 10^4$ and $\alpha = 0.6$ at times (*a*) $\tau = 0.4$, (*b*) $\tau = 0.6$, (*c*) $\tau = 0.7$, (*d*) $\tau = 1.1$.

instead of $r = e^{\lambda z}$ and accordingly the magnification factor is not the same for all times since λ is a function of time. However, they give the general nature of the flow and the appearance of eddies E_1 and E_2 is clearly shown at $\tau = 1.1$.

6. Conclusion

The unsteady flow past an impulsively started rotating and translating circular cylinder has been investigated both theoretically and experimentally for the Reynolds-number range $10^3 \leqslant R \leqslant 10^4$ and for speed ratios up to $\alpha = 3$. A detailed study has been presented for $R = 10^3$. The high-Reynolds-number flow for smaller values of α is characterized by the formation of numerous secondary vortices, unlike the low- or moderate-Reynolds-number cases. It is found from the numerical work that a flow with periodic vortex shedding is established for the lower values of α ($\leqslant$ 2) and this would presumably continue for an indefinitely large time. It has not been possible to study the evolving periodic structure of the flow for a great time in the experiments because of limitations of the apparatus, but over the duration of the study there is an exact correspondence with the calculated flow. When $\alpha = 3$ the situation is slightly different; in this case a vortex system is formed at the surface of the cylinder. One vortex is shed but the vortex remaining in contact with the cylinder surface is swept round to the front of the cylinder where it is rapidly destroyed by the oncoming stream. At this stage the experimental and calculated flows still remain in good agreement, but soon thereafter the experimental flow becomes turbulent while in the calculations there is no further vortex shedding and the flow approaches a steady state. It is of interest to observe that the streamline patterns of the large-time solutions for $\alpha = 3$ (e.g. figure 6*g*, *h*) are quite consistent (taking into account the reversed direction of rotation of the cylinder) with the flow patterns found experimentally in earlier studies, e.g. by Prandtl (1927) (cf. Goldstein 1938, plate 16) for the slightly greater value $\alpha = 4$. They are also of a very similar character to the steady-state solutions found for $\alpha = 1$ at $R = 5, 20$ by Badr *et al.* (1989, pp. 594–595). Finally, the effect of using the boundary-layer limit of the equations of motion rather than the full Navier–Stokes equations at high Reynolds number has been briefly investigated. It is found that the calculations based on the solution of the boundary-layer equations will not give reliable results for the lift and drag unless the effect of pressure is taken into account. Indeed, the boundary-layer solution predicts a lift force which is in the opposite direction to the actual total lift. Thus the boundary-layer simplification of the equations by setting $R = \infty$ cannot be expected to give results at high Reynolds numbers that are consistent with the full Navier–Stokes equations in every respect.

This investigation has been assisted by grants from NATO (No. RG.0416/85) and the Natural Sciences and Engineering Research Council of Canada. Some work was carried out at the Department of Mathematics, University College, London, U.K. by one author (S.C.R.D.) as a Royal Society of London Visiting Research Fellow.

REFERENCES

Badr, H. M., Coutanceau, M., Dennis, S. & Ménard, C. 1985 *C.R. Acad. Sci. Paris* **300**, II, 529.

Badr, H. M., Coutanceau, M., Dennis, S. & Ménard, C. 1986 *C.R. Acad. Sci. Paris* **302**, II, 1127.

Badr, H. M. & Dennis, S. C. R. 1985 *J. Fluid Mech.* **158**, 447.

Badr, H. M. & Dennis, S. C. R. 1987 In *Boundary-Layer Separation* (ed. F. T. Smith & S. Brown), pp. 235–249. Springer.

BADR, H. M., DENNIS, S. C. R. & YOUNG, P. J. S. 1989 *Computers & Fluids* **17**, 579.

BOUARD, R. & COUTANCEAU, M. 1980 *J. Fluid Mech.* **101**, 583.

COLLINS, W. M. & DENNIS, S. C. R. 1973 *J. Fluid Mech.* **60**, 105.

COUTANCEAU, M. & BOUARD, R. 1977 *J. Fluid Mech.* **79**, 231.

COUTANCEAU, M. & MÉNARD, C. 1985 *J. Fluid Mech.* **158**, 399.

DENNIS, S. C. R. & QUARTAPELLE, L. 1989 *Intl J. Numer. Meth. Fluids* **9**, 871.

ECE, M. C., WALKER, J. D. A. & DOLIGALSKI, T. L. 1984 *Phys. Fluids* **27**, 1077.

GLAUERT, M. B. 1957*a* *J. Fluid Mech.* **2**, 89.

GLAUERT, M. B. 1957*b* *Proc. R. Soc. Lond.* A **230**, 108.

GOLDSTEIN, S. 1938 *Modern Developments in Fluid Dynamics*, vol. 1. Oxford University Press.

INGHAM, D. B. 1983 *Computers & Fluids* **11**, 351.

MÉNARD, C. 1984 Étude de la formation du sillage engendré par le démarrage impulsif d'un cylindre soumis à des mouvements combinés de translation et de rotation. Thése de 3$^{me.}$ cycle, Université de Poitiers.

MOORE, D. W. 1957 *J. Fluid Mech.* **2**, 541.

PRANDTL, L. 1927 *J. R. Aero. Soc.* **31**, 736, 737.

PRANDTL, L. & TIETJENS, O. 1931 *Hydro-und-Aeromechanik*, vol. 2. Springer.

TA PHUOC LOC 1975 *J. Méc.* **14**, 109.

WOOD, W. W. 1957 *J. Fluid Mech.* **2**, 77.